Chinese Journal of Chemical Engineering 69 (2024) 13–22

Contents lists available at ScienceDirect

Chinese Journal of Chemical Engineering

journal homepage: www.elsevier.com/locate/CJChE

Full Length Article

Hyperbranched polymer hollow-fiber-composite membranes for pervaporation separation of aromatic/aliphatic hydrocarbon mixtures

Tong Liu [1], Hao Sun [1], Xiangqiong Wang [1], Jie Li [1], Zhanquan Zhang [2], Pei Wu [2], Naixin Wang [1,*], Quanfu An [1]

[1] *Beijing Key Laboratory for Green Catalysis and Separation, Department of Chemical Engineering, College of Materials Science and Engineering, Beijing University of Technology, Beijing 100124, China*
[2] *Petrochemical Research Institute, CNPC, Beijing 102206, China*

ARTICLE INFO

Article history:
Received 18 October 2023
Received in revised form
11 January 2024
Accepted 24 January 2024
Available online 9 February 2024

Keywords:
Aromatic/aliphatic hydrocarbons
Hyperbranched polymer
Pervaporation
Hollow fiber membrane
Dip-coating

ABSTRACT

The separation of aromatic/aliphatic hydrocarbon mixtures is crucial in the petrochemical industry. Pervaporation is regarded as a promising approach for the separation of aromatic compounds from alkanes. Developing membrane materials with efficient separation performance is still the main task since the membrane should provide chemical stability, high permeation flux, and selectivity. In this study, the hyperbranched polymer (HBP) was deposited on the outer surface of a polyvinylidene fluoride (PVDF) hollow-fiber ultrafiltration membrane by a facile dip-coating method. The dip-coating rate, HBP concentration, and thermal cross-linking temperature were regulated to optimize the membrane structure. The obtained HBP/PVDF hollow-fiber-composite membrane had a good separation performance for aromatic/aliphatic hydrocarbon mixtures. For the 50%/50% (mass) toluene/*n*-heptane mixture, the permeation flux of optimized composite membranes could reach 1766 $g \cdot m^{-2} \cdot h^{-1}$, with a separation factor of 4.1 at 60 °C. Therefore, the HBP/PVDF hollow-fiber-composite membrane has great application prospects in the pervaporation separation of aromatic/aliphatic hydrocarbon mixtures.
© 2024 The Chemical Industry and Engineering Society of China, and Chemical Industry Press Co., Ltd. All rights reserved.

1. Introduction

The separation of aromatic/aliphatic hydrocarbon mixtures is of great significance in the petrochemical industry, chemical production, and environmental protection [1–3]. However, the separation of aromatic compounds from alkanes is very difficult due to their similar chemical and physical properties. As an efficient membrane separation technique, pervaporation has great advantages in economy and environment because of its environment-friendly nature, low energy consumption, compact equipment, and easy coupling with other techniques [4–7].

The development of pervaporation membranes depends on their separation performance and its longevity. High-performance polymeric membrane material often requires a complicated synthesis process. The most reported membrane materials for separating mixtures of aromatic and aliphatic hydrocarbons *via* the pervaporation are polymers, such as polyimide, polyurethane, polyacrylate, poly (ether amide), polysiloxane amide, poly (vinyl alcohol), poly (methyl methacrylate), and hyperbranched polymer (HBP) [3,8–17]. They have been widely used because of their effective membrane-forming abilities, functional versatility, and low cost [6,18]. In our previous study, HBP emulsion was prepared in aqueous solution and was then deposited on the surface of a tubular porous ceramic substrate by a negative-pressure-driven assembly method [19]. The green preparation method exhibited excellent application prospects. However, since the HBP was deposited inside the pores of the ceramic tubular porous substrate, the flux of the membrane was only 238 $g \cdot m^{-2} \cdot h^{-1}$, which should be further improved to meet the requirement in the industry. To increase permeation flux, it is necessary to regulate the structure of the HBP-composite membrane.

The membrane module also has a significant influence on the application in industry. Most of the polymers were deposited on the surface of organic flat sheet and ceramic tubular substrate in the field of aromatic/aliphatic separation. Compared with the flat-sheet and tubular membrane modules, the hollow fiber membrane module has the advantage of self-supporting, high packing

* Corresponding author.
E-mail address: wangnx@bjut.edu.cn (N. Wang).

https://doi.org/10.1016/j.cjche.2024.01.009
1004-9541/© 2024 The Chemical Industry and Engineering Society of China, and Chemical Industry Press Co., Ltd. All rights reserved.

density, and ease to scale-up [20]. Therefore, the hollow fiber membrane modules have a promising future in the pervaporation separation industry [21,22]. However, to the best of our knowledge, there are only one report on the fabrication of hollow fiber membrane for the pervaporation separation of aromatic/aliphatic hydrocarbon mixtures [23]. Commercial polybenzimidazole (PBI) and polyimide Matrimid were used to prepare an asymmetric hollow fiber membrane using a non-solvent induced phase separation method. Expanding membrane materials and preparation methods is still the main task. Thin film composite membrane, which is constructed by ultrathin separation layer and porous substrate, has been considered as the promising membrane in industry. However, it is challenging to form an intact and effective separation layer on the three-dimensional substrate surface of hollow fiber.

In this study, an HBP hollow-fiber-composite membrane (HFCM) was prepared for separating aromatic/aliphatic mixtures. A non-ionic, self-emulsifying amphiphilic dendritic polymer HBP was dispersed in water to form an emulsion. The HBP emulsion was deposited on the outer surface of the polyvinylidene fluoride (PVDF) hollow-fiber ultrafiltration membrane by a facile dip-coating method. The stability of the HBP/PVDF HFCM was subsequently improved by thermal cross-linking. The aromatic/aliphatic pervaporation separation performance of the HFCM was optimized by regulating the emulsion concentration, cross-linking temperature, and dip-coating speed. The obtained HBP/PVDF HFCM exhibited an exceptional high flux. This simple, economical, and green preparation process has great potential in industrial applications.

2. Experimental

2.1. Materials

PVDF hollow-fiber membrane (pore size: 120 nm, inner diameter: 0.8 mm, outer diameter: 1.2 mm) was obtained from Tsinghua University. Hyperbranched polymer (HBP, M_w 9000) was provided by Perstorp Specialty Chemicals AB (Sweden). It can be emulsified into emulsion in water only by mechanical stirring without emulsifier or surfactant. Toluene was purchased from Beijing Tongguang Fine Chemical Co. Reagents such as *n*-heptane, cyclohexane, isooctane, and benzene were purchased from Energy Chemical. The deionized water was homemade in the laboratory. All chemicals were used as received without further purification.

2.2. Preparation of HBP/PVDF hollow-fiber-composite membrane

The U-shaped hollow-fiber-membrane module was selected in this study. The hollow-fiber membrane in the U-shaped module could swing with the flowing of the fluid. Then, the relative motion between the fluid and the membrane was increased, which could effectively reduce the concentration polarization.

As shown in Fig. 1, a dip-coating method was used to fabricate the HBP/PVDF HFCM. Firstly, HBP was dispersed in a certain volume of deionized water followed by stirring at 40 °C for 2 h to prepare a clear HBP emulsion. The PVDF hollow-fiber membrane was fixed into a U-shaped module with epoxy resin. Then, the U-shaped PVDF hollow-fiber membrane was dipped into the HBP emulsion using a dip coater. After immersion for a period, the membrane was lifted at a certain speed. The obtained HBP/PVDF HFCM was then subject to thermal cross-linking in an oven at a design temperature.

2.3. Characterizations

Attenuated total reflection Fourier-transform infrared spectroscopy (FTIR, VerTRus-70, Bruker, Germany) was utilized to investigate the evolution of functional groups during thermal cross-linking process. X-ray photoelectron spectroscopy (XPS, Thermo Scientific K-Alpha, America) was utilized to study the elemental composition and chemical bonds on membrane surfaces. Scanning electron microscopy (SEM, Hitachi SU-8020, Japan) was utilized to analyze the morphology of the inner and outer surfaces as well as the cross-section of the hollow-fiber membrane. The roughness of the membrane surface was determined by atomic force microscopy (AFM, Park Systems XE-100). Low-field nuclear magnetic resonance apparatus (LF-NMR, PQ001-010, Niuman Electric Corporation, China) was used to analyze the free-volume variation of thermally cross-linked composite membranes at different temperatures.

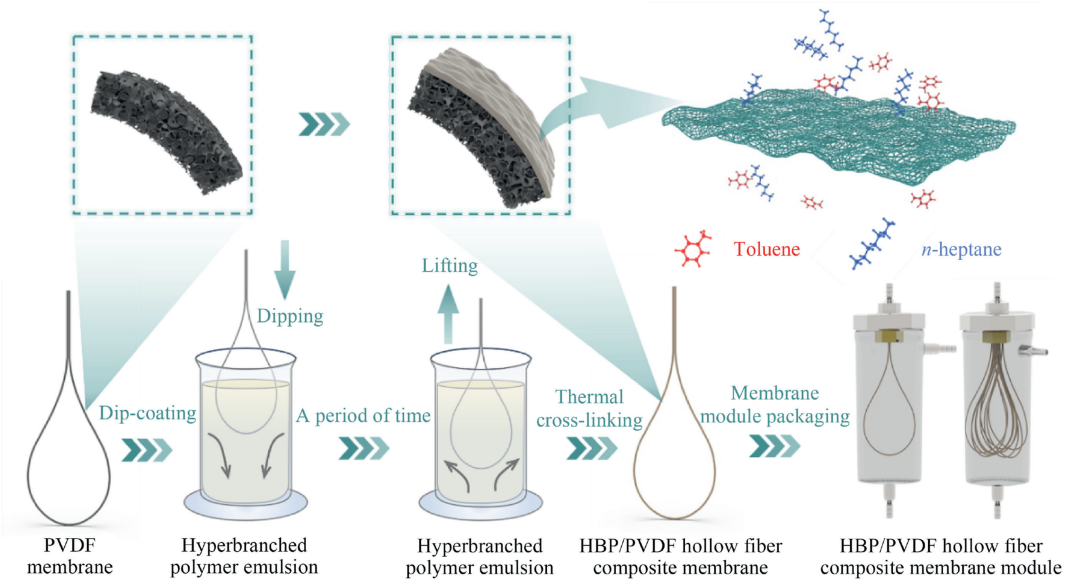

Fig. 1. Schematic illustration of the preparation of HBP/PVDF HFCMs by a dip-coating method.

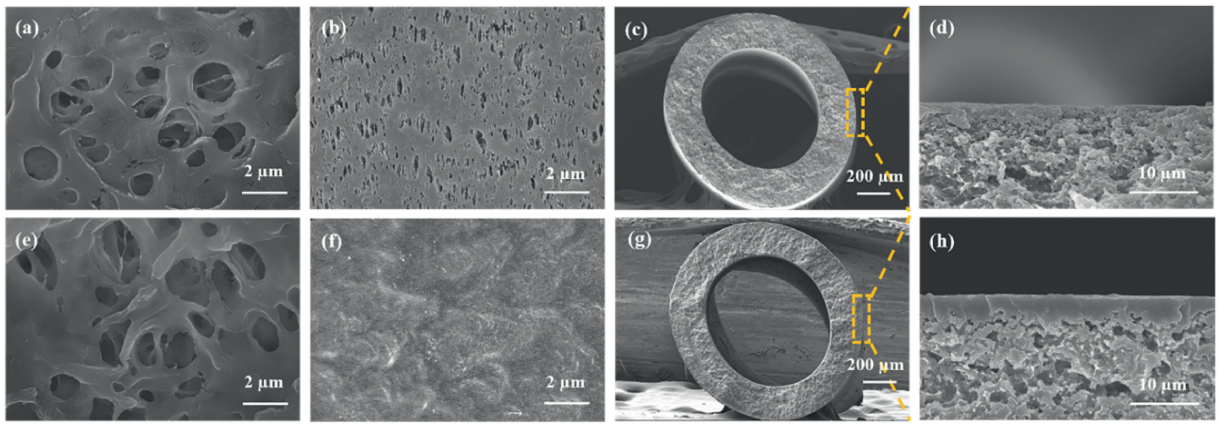

Fig. 2. SEM images of (a) inner surface, (b) outer surface and (c, d) cross sections of PVDF substrate; SEM images of (e) inner surface, (f) outer surface and (g, f) cross sections of HBP/PVDF hollow-fiber-composite membrane. (Preparation conditions: emulsion concentration 20%; dipping time 20 min; lifting rate 5000 $\mu m \cdot s^{-1}$; crosslinking temperature 150 °C; crosslinking time 1 h).

2.4. The measurement of pervaporation performance

The prepared HBP/PVDF HFCM was assembled into a membrane module. The separation performance for the aromatic/aliphatic mixture was tested on a self-made pervaporation device in the laboratory (the effective area of membrane was 10 cm^2). The downstream pressure of the membrane was maintained at 100 Pa. The permeate vapor was collected in a cold trap through liquid nitrogen after pre-running for 40 min. An exact electronic balance was utilized to measure the mass of the permeate. Gas chromatography (FULI GC9790Plus, China, with a hydrogen flame ionization detector, 0.25 mm × 30 m Agilent DB-624 capillary column) was utilized to examine the composition of the gathered samples. The injection temperature, column temperature, and detector temperature were 120 °C, 150 °C and 180 °C, respectively. For accuracy, each test was finished at least three times.

The pervaporation performance of the HBP/PVDF hollow-fiber membrane was evaluated by the permeation flux (J) and the separation factor (β) as follows:

$$J = \frac{Q}{A \times t} \tag{1}$$

where J is the permeate flux ($g \cdot m^{-2} \cdot h^{-1}$); Q is the mass of the permeate (g); t is the permeation time (h); A is the effective area of the membrane (m^2).

$$\beta_{i/j} = \frac{y_i / y_j}{x_i / x_j} \tag{2}$$

where β is the separation factor; y_i and y_j are the mass fraction (%) of components i and j in the permeate, respectively; x_i and x_j are the mass fractions of components i and j in the feed (%), respectively.

3. Results and Discussion

3.1. Characterization of the HBP/PVDF composite membranes

3.1.1. Characterization of membrane morphology

To figure out whether the separation layer of HBP was uniformly coated onto the outer layer of the PVDF substrate, the characterization of SEM was used for the surface and cross-sectional morphology. As shown in Fig. 2, the outer and inner diameters of the PVDF substrate were 1.2 mm and 0.8 mm, respectively, with sponge-like pore texture inside the membrane. The irregular pores were found on the outer surface with an average pore diameter of 0.12 μm, whereas the pores in a micrometer scale were found on the inner surface. When the PVDF substrate was dip-coated by HBP, it could be clearly seen that a dense separation layer was formed. Moreover, it can also be seen from the cross section that some HBP penetrated into the pores of the hollow-fiber substrate. Therefore, the HBP separation layer could not be easily peeled off from the substrate to obtain a good combination with the support layer. The HBP separation layer has a thickness of about 4 μm.

AFM was utilized to measure the outer surface roughness of the PVDF substrate and the HBP/PVDF HFCM. As shown in Fig. 3, The roughness (Ra) value of the PVDF substrate was about 43.4 nm. As for the HBP/PVDF, the surface roughness of the HFCM was decreased to around 27.4 nm, demonstrating the formation of a homogeneous HBP separation layer on the substrate. This is due to the presence of large pore structures on the PVDF substrate, whereas a smooth and continuous separation layer is formed on the surface of the HFCM.

3.1.2. Effect of preparation conditions on membrane morphology

Studies have shown that the synthetic conditions during membrane preparation have a great influence on the morphology, thickness, pore size, as well as its separation performance. One of the significant factors influencing membrane thickness is the concentration of the emulsion. The cross-sectional morphology of the HFCMs with different emulsion concentrations was characterized by SEM. As shown in Fig. 4, with the increase of the polymer emulsion concentration, the separation layer gradually became thicker, which was mainly related to the increase of the emulsion viscosity (the corresponding viscosities of emulsions with different concentrations at 25 °C are shown in Table. S1 in Supplementary Material) and the decrease of the particle size of the HBP emulsion [19]. High viscosity will lead to the increase of the adhesion force between the HBP and PVDF substrate.

The morphology of the membrane is also influenced by the dipping and lifting rate. As shown in Fig. 5, the cross-sectional morphologies of the HFCMs with different lifting rates (1000–13000 $\mu m \cdot s^{-1}$) were compared. Moreover, the uniformity of the separation-layer thickness throughout the fiber has a significant influence on the separation performance of the membrane. Consequently, the thickness of the separation layer at different regions was also investigated. Two regions including region I with a small curvature and region II with a larger curvature were selected.

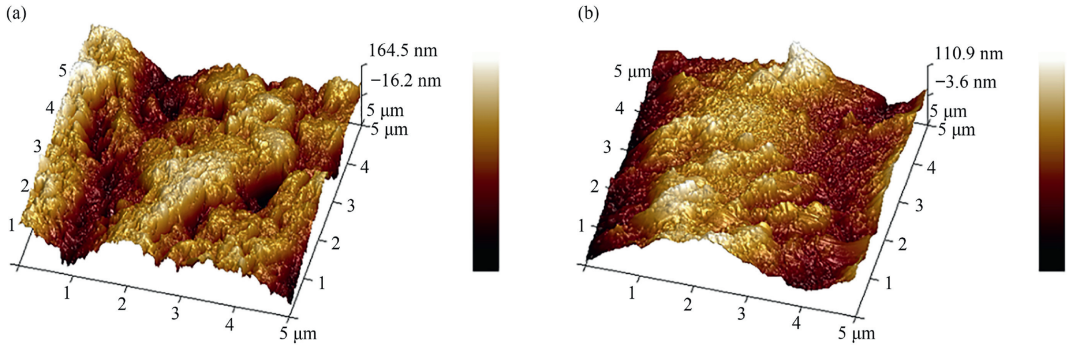

Fig. 3. The AFM images of the outer surface of (a) PVDF substrate and (b) HBP/PVDF HFCM.

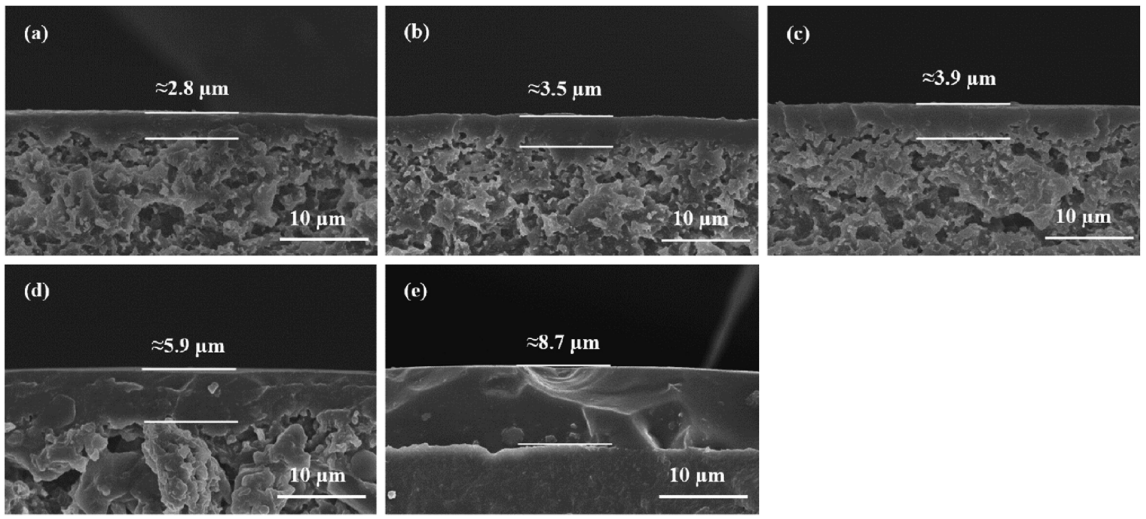

Fig. 4. SEM images of the cross-sectional morphologies of the HBP/PVDF HFCMs with the concentration of HBP emulsion of (a) 10%, (b) 15%, (c) 20%, (d) 25%, (e) 35%.

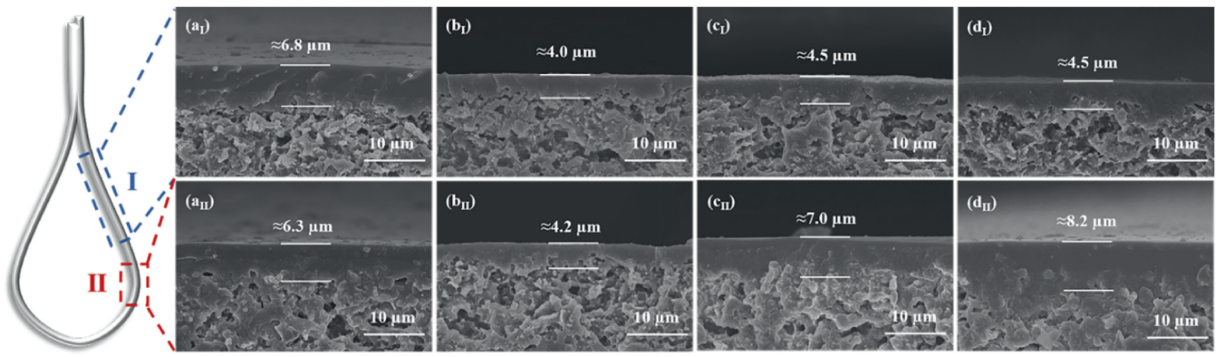

Fig. 5. SEM images of the cross-section morphology of HBP/PVDF HFCMs at different regions with lifting speed of (a) 1000 μm·s^{-1}, (b) 5000 μm·s^{-1}, (c) 9000 μm·s^{-1}, (d) 13000 μm·s^{-1}.

When the lifting rate was 1000 μm·s^{-1}, the thickness of the separation layer in the region I and II were about 6.8 and 6.3 μm, respectively. When the lifting rate was up to 5000 μm·s^{-1}, the thickness of the separation layer in the two regions was about 4.0 and 4.2 μm, respectively. It was the reason that the high speed could increase the shear force on the membrane surface. However, as the lifting rate further reached 13000 μm·s^{-1}, the thickness of the separation layer on region I had no obvious change, whereas the thickness on region II was increased. It indicated that the excessive lifting speed was helpless in enhancing the shear force, but it could result in the formation of a nonuniform thickness. Therefore, 5000 μm·s^{-1} was the optimal lifting speed to prepare the HBP/PVDF HFCMs.

3.1.3. FTIR and XPS characterization of the membrane

FTIR spectra were used to characterize the functional groups on the PVDF substrate, HBP, and HBP/PVDF HFCMs. As shown in Fig. 6(a), the peaks at 3510 cm^{-1} and 1120 cm^{-1} were attributed to the ν_s (OH) (large broad peak) and ν_{as} (C—OH) absorption peaks in PEG chain segments in HBP [19]. The two peaks near 2900 cm^{-1} were the coupling of the ν (OH) absorption peaks of carboxylic acid with the ν_s (CH) and ν_{as} (CH) absorption peaks of —CH_2—. The

adsorption peaks of ν (C=O) and σ (OH) in the carboxyl group were observed at 1740 cm^{-1} and 1460 cm^{-1}, respectively. These peaks could also be clearly seen on the HBP/PVDF HFCMs. In addition, the elemental composition and chemical state of the membrane surface were further studied using XPS. As shown in Fig. 3(c), the two peaks of binding energy at 687.8 eV and 285.9 eV were the F 1s and C 1s peaks on the PVDF substrate, respectively. The peaks at 532.2 eV and 285.9 eV on the HBP/PVDF membrane were attributed to O 1s and C 1s, respectively, in the HBP. The O 1s peak from HBP could be seen on the HBP/PVDF HFCMs [24]. These results indicate that the HBP membrane was successfully prepared on the PVDF substrate. As shown in Fig. 3(d) and (e), the C 1s and O 1s high-resolution spectra of HBP/PVDF membranes were also analyzed. The XPS of C 1s could be deconvoluted into three peaks, which belong to C—C/C=C (284.8 eV), C—O (286.3 eV), and C=O (289.0 eV) [25–27]. The XPS of O 1s could be deconvoluted into two peaks, attributed to C—O (531.8 eV) and C—O (533.0 eV) [28,29]. These chemical bonds were from unsaturated fatty acids and polyethylene glycol chains in HBP. Due to the presence of hydrophilic groups —COOH and —OH in the polymer chain, the water contact angle of the HBP/PVDF HFCM was smaller than that of the PVDF substrate membrane (Fig. S1).

The HBP crosslinked at various temperatures was also characterized using FTIR spectra to investigate the cross-linking procedure of the HBP. As shown in Fig. 6(b), with the increase of crosslinking temperature, the absorption peak ν (OH) at 2900 cm^{-1} was shifted and the peak intensity was decreased, indicating that chemical crosslinking of the group causes the reduction of —OH in the PEG chain. The shift of the ν (C=O) absorption peak at 1740 cm^{-1}, which is attributed to the formed ester groups, were formed due to high chemical cross-linking with the increased temperature, and the electron induction of C=O was weaker for $—O^-$ than that for —OH. Therefore, the absorption peak was shifted to the place with a small wave number. In addition, a new absorption peak ν (COC) at 1000–1300 cm^{-1} was observed for the ester group generated from chemical cross-linking, leading to a shift of the absorption peak at 1120 cm^{-1}. Subsequently, ^{13}C NMR spectroscopy was tested before and after cross-linking of HBP (Fig. S2). The characterization results of FTIR spectra and ^{13}C NMR spectroscopy both indicated that after thermal cross-linking at different temperatures, —OH and —COOH on the HBP chain segment reacted with each other to form a dense separation layer.

3.1.4. LF-NMR characterization of the membrane

In the LF-NMR technique, the time required for the nucleus of ^1H to return from the excited state to the equilibrium state is the relaxation time. Here, T_2 is the spin-spin or transverse relaxation time. In this study, the signal of NMR was mainly expressed by T_2 relaxation time. The amount of hydrogen protons in the membrane or solvent can be reflected by the relative peak intensity of the T_2 signal peak. The temporal shift of T_2 can be utilized to infer the alteration of the free space between the polymer chains in the membrane. First, the affinity of HBP for aromatic and aliphatic molecules was determined by studying the spin-spin relaxation time T_2 of ^1H in different solvents [30]. Fig. 7(a) shows the LF-NMR signal of HBP/PVDF HFCMs in toluene and *n*-heptane. The signal peak during the high relaxation period (the peak at the far right) is the ^1H signal peak T_{2l} in the free solvent molecule. However, the signal peak less than 10^3 ms is the ^1H signal peak T_{2a} of the adsorbed solvent molecules between polymer chains or within pores inside the membrane. It can be seen that the ratio of the T_{2a} signal intensity to the total signal intensity (T_{2l}+T_{2a}) in toluene is significantly higher than that in *n*-heptane, which indicates that the HBP/PVDF HFCMs have a stronger affinity for toluene [31,32]. To exclude the influence of the macro-pore structure in the PVDF substrate on the results, the HBP was tested by LF-NMR. As shown in Fig. 7(b), a similar result was obtained, that is, the HBP has a stronger adsorption of toluene than that of *n*-heptane.

The crosslinking temperature is an important factor that affects the polymer chain structure. Therefore, LR-NMR was used to systematically analyze the polymer chain segments in the membranes with different crosslinking temperatures. As shown in Fig. 7(c), the polymer chain segment can be divided into two regions according to the degree of restriction [33]. Region I is a low-degree-of-freedom region with a relaxation time of 0.1–1 ms, in which the peak is the 1H signal peak near the crosslinking and entanglement

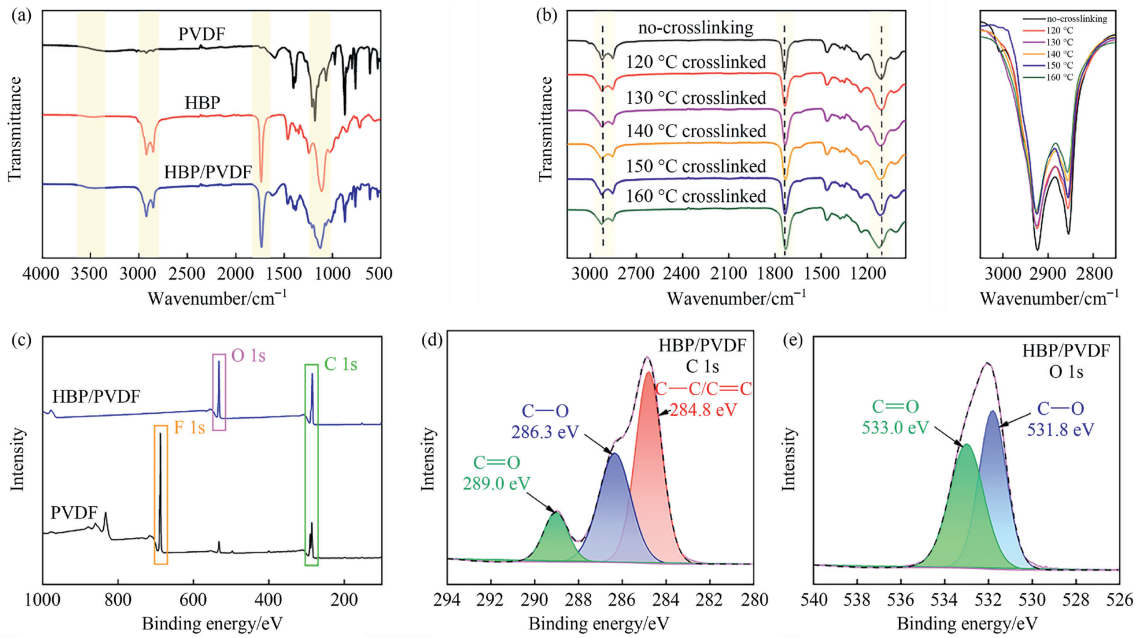

Fig. 6. FTIR spectra of (a) PVDF substrate, HBP, HBP/PVDF HFCMs, and (b) crosslinked HBP at different temperatures. (c) XPS survey spectra of PVDF substrate and HBP/PVDF HFCMs, high-resolution spectra of (d) C 1s, (e) O 1s.

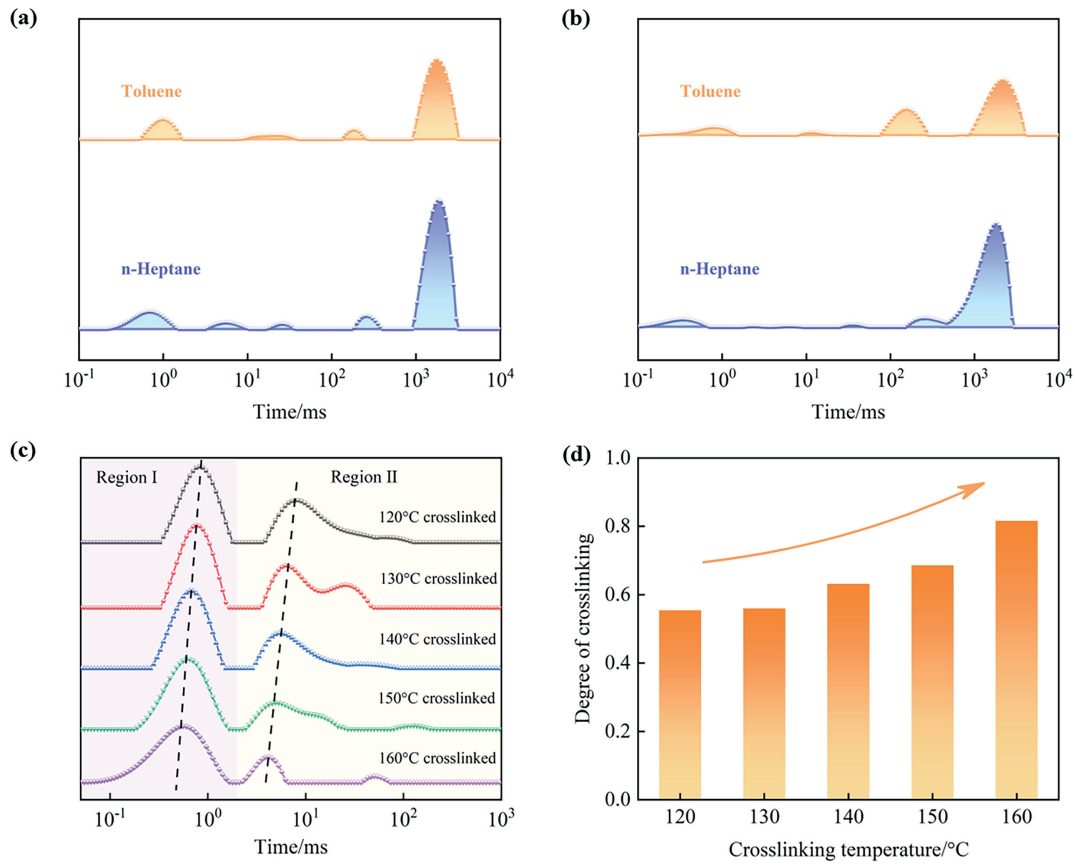

Fig. 7. LF-NMR signals of (a) HBP/PVDF HFCMs and (b) HBP in toluene and *n*-heptane; (c) LF-NMR relaxation spectra and (d) crosslinking degree of HBP/PVDF HFCMs prepared at different crosslinking temperatures.

points of the hyperbranched polymer chain. Region II is a high-degree-of-freedom region with relaxation time between 1 and 100 ms, where the peaks are the ^{1}H signal peaks of the partial crosslinked suspended tail chain and the uncrosslinked free chain. As the cross-linking temperature increases, the peak in Region I shifts to the left, demonstrating that the degree of cross-linking increases; as such, the free volume seen in the polymer chain decreases. The same trend also appears in Region II, which indicates that the polymer chains with incomplete cross-linking also gradually tend to be crosslinked with the increase of temperature, and the distance of the free volume between the chains decreases. As the cross-linking temperature increases, the cross-linking efficiency increases, so the ^{1}H signal peaks on the suspended tail chain and the free chain in region II are gradually separated. By calculating the ratio of the ^{1}H signal peak to the total peak area on the crosslinked chain, the crosslinking degree of the membrane with different crosslinking temperatures can be obtained [34]. As shown in Fig. 7(d), the crosslinking degree gradually increases as the crosslinking temperature rises. Therefore, the cross-linking temperature can be modified to alter the free volume and degree of crosslinking of the membrane, hence regulating the transport efficiency in the pervaporation process.

3.2. Effects of membranes preparation conditions on the separation performance

The as-prepared HBP/PVDF HFCMs were utilized in the pervaporation separation of aromatic/aliphatic hydrocarbon mixtures. On the one hand, the benzene ring on aromatic hydrocarbons has an indefinite domain distribution of p-orbital electrons, which are prone to polarization upon induction by polar groups. However, HBP contains polar groups —OH and —COOH, which will cause strong interaction between the polymer and the groups of the polarized aromatic compounds, relax the polymer chain, and promote the mass transfer of aromatic compounds in the membrane material [17,35]. In addition, the benzene ring contains a π electronic structure, whereas the unsaturated bond in HBP has a π-electron acceptor unit. Therefore, HBP can interact with aromatic compounds by π-π stacking [36,37]. The performance of pervaporation membrane mainly depends on the properties of membrane materials, membrane structure, and the interaction between membrane and pervaporation components. The permeation flux of the components through the composite membrane is proportional to the permeability and driving force and inversely proportional to the membrane thickness [6]. The permeability of the components is related to the adsorption processes occurring on the membrane surface and the diffusion processes occurring within the main body of the membrane (details are provided in the calculation of membrane permeability section in the Supplementary Material). When the thickness of the membrane increases, or the free volume of the polymer decreases, the mass transfer resistance of the membrane will increase. Then, the mass of the permeate (Q) in Eq. (1) will be reduced, resulting in the decrease of the membrane permeation flux (J). At the same time, it will also increase the permeability through component, that is, the increase of y_i in Eq. (2), which will increase the separation factor (β). Therefore, the free volume, thickness, and uniformity of the membrane should be regulated to obtain the optimal membrane preparation conditions. In this study, a 50% toluene/*n*-heptane mixture was used to evaluate the separation performance of the membrane.

3.2.1. Effect of polymer emulsion concentration

As shown in Fig. 8, the effect of the emulsion concentration on the separation performance was investigated. The flux of the HFCM declined from 569 to 98 $g \cdot m^{-2} \cdot h^{-1}$ as the concentration of HBP emulsion increased from 10% to 35% (mass), and the greatest value of separation factor was found at a concentration of 20% (mass). This is due to the increasing thickness of the separation layer with increasing emulsion concentration (Fig. 4). Thus, the transport resistance of the membrane was increased, resulting in a decrease in flux. On the one hand, too thick a separation layer can lead to reduced membrane-forming ability of HBP. On the other hand, the increase of emulsion concentration leads to excessive viscosity, and more emulsion is accumulated where the curvature of the membrane fiber is large (*i.e.*, region II in Fig. 5), which makes the separation layer start to become uneven, leading to a decrease of the separation factor. Consequently, 20% (mass) was selected as the optimal concentration.

3.2.2. Effect of crosslinking temperature

The thermal crosslinking temperature has an influence on the behavior of chains to change the free volume and crosslinking degree of the membrane [38]. Therefore, the effect of crosslinking temperature on the separation performance was investigated in this study. As shown in Fig. 9, the separation factor of the membranes increased from 1.98 to 4.93, whereas the permeation flux decreased from 3328 to 53 $g \cdot m^{-2} \cdot h^{-1}$ with the increase of crosslinking temperature. It is postulated that the increase of crosslinking temperature could promote the entanglement and group cross-linking between polymer chains, which not only increases the cross-linking degree but also reduces the free volume of polymer chains, constraining the movement of polymer chains. Consequently, the permeation flux was reduced with the increasing of separation factor. The membrane can achieve optimal performance at a temperature of 150 °C.

3.2.3. Effect of dip-coating speed

In this study, the dip-coating technique was used to prepare the HFCMs. Consequently, the structure and characteristics of the composite membrane are greatly influenced by the lifting speed. If the lifting rate is too slow, a large amount of emulsion will be accumulated on the membrane surface to increase the thickness of the separation layer (Fig. 5(a)). However, if the lifting speed was too fast, the non-uniform separation layer would deteriorate the separation performance (Fig. 5(d)). As shown in Fig. 10, when the lifting speed increased from 1000 to 13000 $\mu m \cdot s^{-1}$, the separation factor decreased from 4.6 to 2.9, whereas the flux increased first and then decreased. When the lifting speed was 5000 $\mu m \cdot s^{-1}$, the separation factor of the HFCM was 4.2, with a flux of 382 $g \cdot m^{-2} \cdot h^{-1}$ for separating 50% (mass) toluene/*n*-heptane mixtures.

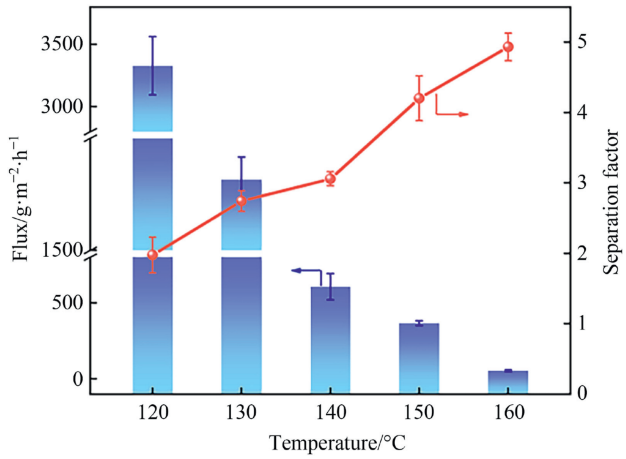

Fig. 9. Effects of crosslinking temperature on permeation flux and separation factor of HFCMs. (Preparation conditions: emulsion concentration 20%; dipping time 20 min; lifting rate 5000 $\mu m \cdot s^{-1}$; crosslinking time 1 h. Operating conditions: feed temperature 40 °C; 50% (mass) toluene/*n*-heptane solution).

3.3. Effects of operation process on the separation performance

During the pervaporation process, the operation process also has a significant influence on the separation performance due to its effect on diffusion coefficient and driving force from concentration difference. In this study, the effects of feed concentration and temperature on the separation performance were investigated. As shown in Fig. 11(a), with the toluene concentration increased from 10% to 50% (mass), the flux was increased from 34 $g \cdot m^{-2} \cdot h^{-1}$ to 382 $g \cdot m^{-2} \cdot h^{-1}$, whereas the separation factor decreased from 5.8 to 4.2. As the toluene concentration in the feed increased, the partial pressure difference of toluene across the membrane was

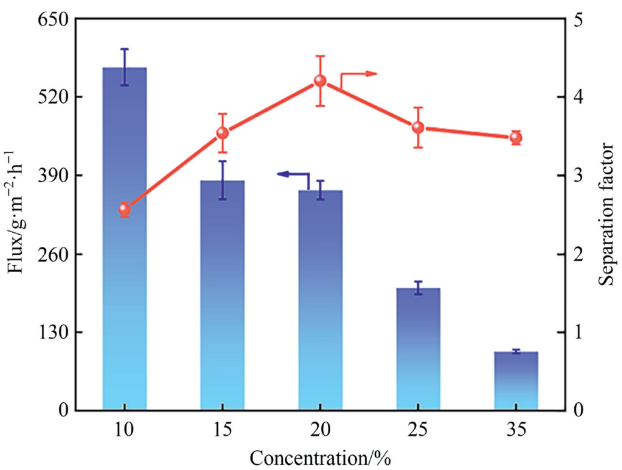

Fig. 8. Effects of HBP concentration on permeation flux and separation factor of HFCMs. (Preparation conditions: dipping time 20 min; lifting rate 5000 $\mu m \cdot s^{-1}$; crosslinking temperature 150 °C; crosslinking time 1 h. Operating conditions: feed temperature 40 °C 50% (mass) toluene/*n*-heptane solution).

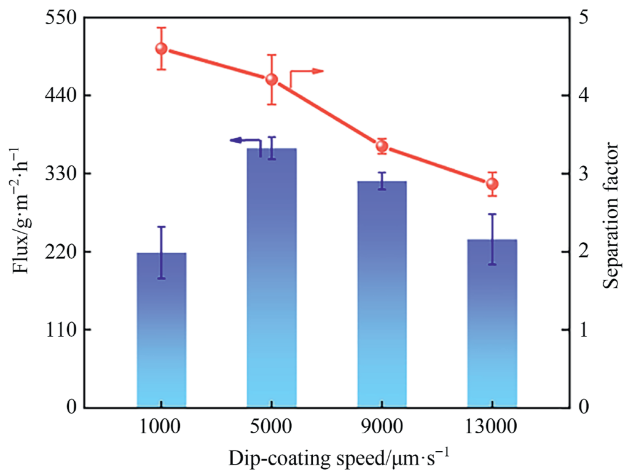

Fig. 10. Effects of lifting speed on permeation flux and separation factor of HFCMs. (Preparation conditions: emulsion concentration 20%; dipping time 20 min; crosslinking temperature 150 °C; crosslinking time 1 h. Operating conditions: feed temperature 40 °C; 50% (mass) toluene/*n*-heptane solution).

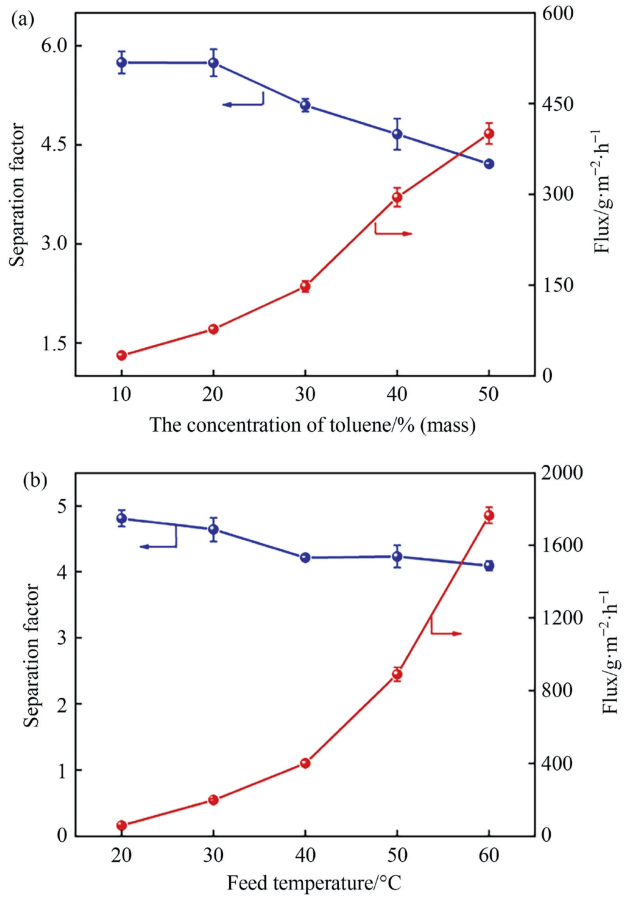

Fig. 11. Effects of (a) feed concentration and (b) feed temperature on the pervaporation performance of HBP/PVDF HFCMs. (Preparation condition: emulsion concentration 20%; dipping time 20 min; crosslinking temperature 150 °C; crosslinking time 1 h; lifting rate 5000 μm·s^{-1}).

improved to increase the flux. Secondly, the increase of aromatic hydrocarbons in the feed caused the membrane to swell due to its affinity of aromatics, which enhanced the mobility of the polymer chain [39] and promoted the penetration of aromatic and aliphatic molecules. For a 50% mixture of toluene and *n*-heptane, the separation factor of HFCM was around 4.2 and its permeation flux was 382 g·m^{-2}·h^{-1}.

Subsequently, the effect of the feed temperature on the pervaporation performance was investigated. As shown in Fig. 11(b), as the feed temperature increased from 20 °C to 60 °C, the permeation flux increased sharply from 60 to 1766 g·m^{-2}·h^{-1}, whereas the separation factor decreased slightly from 4.8 to 4.1. This is because the partial vapor pressure of the permeating molecules is temperature-dependent. High temperatures will increase the degree of random thermal motion of the permeating molecules. In addition, the decrease in the separation factor indicated that the *n*-heptane molecules permeate slightly faster than the toluene molecules. In summary, the rise in flux caused by the increased temperature is much greater than the decrease in selectivity. This indicated that the HBP/PVDF HFCM has a strong practical application for aromatic/aliphatic compounds' separation at high temperatures.

3.4. Comparison of membrane pervaporation performance and membrane stability

In addition to the separation of toluene/*n*-heptane mixtures, other aromatics/aliphatic compounds with similar boiling points were also discussed. The results showed that the HBP/PVDF HFCM had a good pervaporation performance for separating benzene/cyclohexane, toluene/cyclohexane, and toluene/cyclohexane mixtures (Fig. 12(a)). The membrane had a high flux for separating the benzene/cyclohexane mixture because the molecular dynamic diameter of benzene and cyclohexane was small. For the toluene/*iso*-octane mixture, the separation factor was increased due to the larger spatial structure of *iso*-octane than that of *n*-heptane.

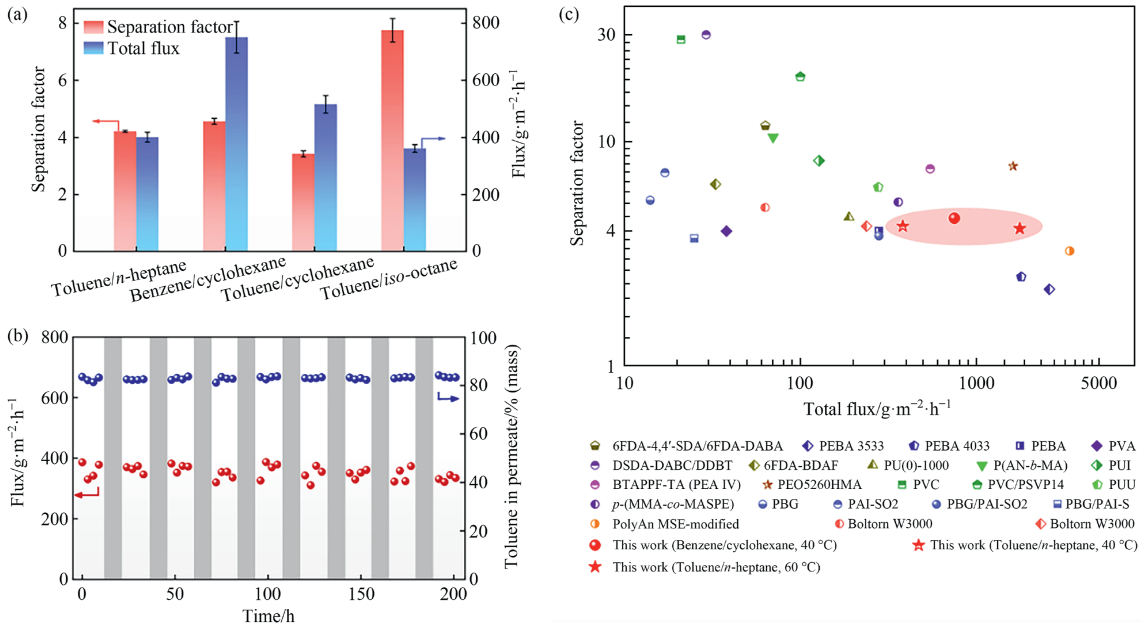

Fig. 12. (a) Pervaporation performance of HBP/PVDF HFCMs for separation of various aromatic/aliphatic mixtures at 40 °C; (b) stability of HBP/PVDF HFCMs (Synthetic condition: emulsion concentration 20%; crosslinking temperature 150 °C; crosslinking time 1 h; lifting rate 5000 μm·s^{-1}. Operating conditions: 50% (mass) toluene/*n*-heptane solution; feed temperature 40 °C); (c) comparison of separation performance of HBP/PVDF HFCM and other membrane reported (Feed fluid composition is listed in Table S2 of the Supplementary Material).

According to these findings, the prepared HBP/PVDF HFCMs are a good candidate for the practical application of pervaporation separation of aromatic and aliphatic mixtures.

The stability and longevity of the membrane is a key factor in practical industrial applications. In this study, the separation performance of the HBP/PVDF HFCMs was evaluated for 210 h. According to Fig. 12(b), the permeation flux of the membrane can be maintained between 330 and 390 $g \cdot m^{-2} \cdot h^{-1}$ along with the toluene concentration of the permeate about 82%. It indicated that the composite membrane showed an excellent swelling resistance, which was due to the penetration of HBP in the substrate pore and the thermal crosslinking, forming a stable network structure. The separation performance of the HBP/PVDF HFCM was compared with those of other membranes reported. The HBP/PVDF HFCM had an excellent flux with a comparable separation factor (Fig. 12(c)). Considering the advantage of hollow-fiber-membrane module, the obtained HBP/PVDF HFCM may have broad application prospects in the practical application.

4. Conclusions

In this study, an HBP/PVDF HFCM was successfully prepared by a facile dip-coating method. The composite membrane was subject to thermal crosslinking with the enhancement of the separation performance and stability. The uniformity of the separation-layer thickness throughout the fiber was regulated through controlling the lifting rate. Finally, a 4-μm-thick HBP separation layer was fabricated on the outer surface of the PVDF hollow-fiber membrane. The obtained HBP/PVDF HFCM exhibited remarkable separation performance in the separation of aromatic and aliphatic mixtures, achieving an excellent flux of 1766 $g \cdot m^{-2} \cdot h^{-1}$ for the 50%/50% (mass) toluene/*n*-heptane mixture at 60 °C.

CRediT Authorship Contribution Statement

Tong Liu: Investigation, Methodology, Data Curation, Formal analysis, Validation, Writing — Original Draft. **Hao Sun**: Formal analysis. **Xiangqiong Wang**: Formal analysis. **Jie Li**: Formal analysis. **Zhanquan Zhang**: Investigation, Formal analysis, Writing — Reviewing and Editing. **Pei Wu**: Formal analysis, Funding acquisition. **Naixin Wang**: Investigation, Formal analysis, Project administration, Supervision, Writing — Reviewing and Editing, Funding acquisition. **Quan-Fu An**: Investigation, Project administration, Supervision, Funding acquisition.

Declaration of Interest

The authors declare that they have no known competing financial interests or personal relationships that could have appeared to influence the work reported in this paper.

Data Availability

All data that support the findings of this study are included in this manuscript and its supplementary information files.

Acknowledgements

This work was financially supported by the National Natural Science Foundation of China (22178008, 22125801) and Petrochina (2022DJ6004).

Supplementary Material

Supplementary data to this article can be found online at https://doi.org/10.1016/j.cjche.2024.01.009.

References

[1] J.P. Garcia Villaluenga, A. Tabe-Mohammadi, A review on the separation of benzene/cyclohexane mixtures by pervaporation processes, *J. Membr. Sci.* 169 (2) (2000) 159–174.
[2] T. Xi, L. Tang, W.T. Hao, L.L. Yao, P. Cui, Morphology and pervaporation performance of ionic liquid and waterborne polyurethane composite membranes, *RSC Adv.* 8 (14) (2018) 7792–7799.
[3] T. Wu, N.X. Wang, J. Li, L. Wang, W. Zhang, G.J. Zhang, S.L. Ji, Tubular thermal crosslinked-PEBA/ceramic membrane for aromatic/aliphatic pervaporation, *J. Membr. Sci.* 486 (2015) 1–9.
[4] X.S. Feng, R.Y.M. Huang, Liquid separation by membrane pervaporation: A review, *Ind. Eng. Chem. Res.* 36 (4) (1997) 1048–1066.
[5] P.V. Naik, S. Kerkhofs, J.A. Martens, I.F.J. Vankelecom, PDMS mixed matrix membranes containing hollow silicalite sphere for ethanol/water separation by pervaporation, *J. Membr. Sci.* 502 (2016) 48–56.
[6] G.P. Liu, W.Q. Jin, Pervaporation membrane materials: Recent trends and perspectives, *J. Membr. Sci.* 636 (2021) 119557.
[7] L.H. Xu, Y. Li, S.H. Li, M.Y. Lv, Z.P. Zhao, Space-confined growth of 2D MOF sheets between GO layers at room temperature for superior PDMS membrane-based ester/water separation, *J. Membr. Sci.* 656 (2022) 120605.
[8] M.T.H. Suding, C. Staudt, Sulfur-containing copolyimides for the membrane-based separation of aromatic/aliphatic mixtures, *J. Appl. Polym. Sci.* 127 (6) (2013) 5065–5074.
[9] S. Maji, S. Banerjee, Synthesis and characterization of new meta connecting semifluorinated poly(ether amide)s and their pervaporation properties for benzene/cyclohexane mixtures, *J. Membr. Sci.* 360 (1–2) (2010) 380–388.
[10] A.E. Yildirim, N.D. Hilmioglu, S. Tulbentci, Separation of benzene/cyclohexane mixtures by pervaporation using PEBA membranes, *Desalination* 219 (1–3) (2008) 14–25.
[11] A. Wolińska-Grabczyk, Effect of the hard segment domains on the permeation and separation ability of the polyurethane-based membranes in benzene/cyclohexane separation by pervaporation, *J. Membr. Sci.* 282 (1–2) (2006) 225–236.
[12] H.H. Schwarz, G. Malsch, Polyelectrolyte membranes for aromatic–aliphatic hydrocarbon separation by pervaporation, *J. Membr. Sci.* 247 (1–2) (2005) 143–152.
[13] Q.F. An, J.W. Qian, Q. Zhao, C.J. Gao, Polyacrylonitrile-block-poly(methyl acrylate) membranes 2: Swelling behavior and pervaporation performance for separating benzene/cyclohexane, *J. Membr. Sci.* 313 (1–2) (2008) 60–67.
[14] M. Iravaninia, M. Mirfendereski, T. Mohammadi, Pervaporation separation of toluene/*n*-heptane mixtures using a MSE-modified membrane: Effects of operating conditions, *Chem. Eng. Res. Des.* 90 (3) (2012) 397–408.
[15] T. Aouak, A. Ali Alghamdi, A.A. Alrashdi, M. Ouladsmane, M.M. Alam, Z. AlOthman, M. Naushad, Miscibility enhancement of poly(vinyl chloride)/polystyrene blend: Application to membrane separation of benzene from benzene/cyclohexane mixture by pervaporation, *Sep. Sci. Technol.* 51 (14) (2016) 2440–2454.
[16] Y. Zhang, N.X. Wang, S.L. Ji, R. Zhang, C. Zhao, J.R. Li, Metal–organic framework/poly(vinyl alcohol) nanohybrid membrane for the pervaporation of toluene/*n*-heptane mixtures, *J. Membr. Sci.* 489 (2015) 144–152.
[17] N.X. Wang, L. Wang, R. Zhang, J. Li, C. Zhao, T. Wu, S.L. Ji, Highly stable "pore-filling" tubular composite membrane by self-crosslinkable hyperbranched polymers for toluene/*n*-heptane separation, *J. Membr. Sci.* 474 (2015) 263–272.
[18] H.X. Liu, N.X. Wang, C. Zhao, S.L. Ji, J.R. Li, Membrane materials in the pervaporation separation of aromatic/aliphatic hydrocarbon mixtures—A review, *Chin. J. Chem. Eng.* 26 (1) (2018) 1–16.
[19] N.X. Wang, T. Wu, L. Wang, X.T. Li, C. Zhao, J. Li, S.L. Ji, Hyperbranched polymer composite membrane using water as solvent for separating aromatic/aliphatic hydrocarbon mixtures, *Sep. Purif. Technol.* 179 (2017) 225–235.
[20] C.F. Wan, T.S. Yang, G.G. Lipscomb, D.J. Stookey, T.S. Chung, Design and fabrication of hollow fiber membrane modules, *J. Membr. Sci.* 538 (2017) 96–107.
[21] W.M. Liu, H. Mao, Y.J. Wang, S.H. Li, Y.N. Feng, L.H. Xu, S. Wang, C. Pei, Z.P. Zhao, Fabrication of highly permeable PDMS@ZIF-8/PVDF hollow fiber composite membrane in module for ethanol-water separation, *AIChE. J.* 69 (9) (2023) e18120.
[22] S.Y. Pang, Z.H. Si, Y. Zhuang, H.Z. Wu, J. Baeyens, X.M. Zhang, P.Y. Qin, Photocured fabrication of PDMS hollow fiber membrane for the pervaporative separation of 1-butanol from water, *Sep. Purif. Technol.* 319 (2023) 123978.
[23] G. Kung, L.Y. Jiang, Y. Wang, T.S. Chung, Asymmetric hollow fibers by polyimide and polybenzimidazole blends for toluene/*iso*-octane separation, *J. Membr. Sci.* 360 (1–2) (2010) 303–314.
[24] L.S. Zhu, X.X. Guo, Y.Q. Chen, Z. Chen, Y.H. Lan, Y.B. Hong, W.G. Lan, Graphene oxide composite membranes for water purification, *ACS Appl. Nano Mater.* 5 (3) (2022) 3643–3653.
[25] J.H. Liu, Q. Yu, M. Yu, S.M. Li, K. Zhao, B. Xue, H. Zu, Silane modification of titanium dioxide-decorated graphene oxide nanocomposite for enhancing

anticorrosion performance of epoxy coatings on AA-2024, *J. Alloys Compd.* 744 (2018) 728–739.
[26] A.V. Shchukarev, D.V. Korolkov, XPS Study of group IA carbonates, *Cent. Eur. J. Chem.* 2 (2) (2004) 347–362.
[27] E.A. Chernova, D.I. Petukhov, A.P. Chumakov, A.V. Kirianova, I.S. Sadilov, O.O. Kapitanova, O.V. Boytsova, R.G. Valeev, S.V. Roth, A.A. Eliseev, A.A. Eliseev, The role of oxidation level in mass-transport properties and dehumidification performance of graphene oxide membranes, *Carbon* 183 (2021) 404–414.
[28] H. Nohira, W. Tsai, W. Besling, E. Young, J. Petry, T. Conard, W. Vandervorst, S. De Gendt, M. Heyns, J. Maes, M. Tuominen, Characterization of ALCVD-Al_2O_3 and ZrO_2 layer using X-ray photoelectron spectroscopy, *J. Non-Cryst. Solids* 303 (1) (2002) 83–87.
[29] W. Wang, X. Wang, Y. Pan, K.M. Liew, O.A. Mohamed, L. Song, Y. Hu, Synthesis of phosphorylated graphene oxide based multilayer coating: Self-assembly method and application for improving the fire safety of cotton fabrics, *Ind. Eng. Chem. Res.* 56 (23) (2017) 6664–6670.
[30] L.L. Zhang, L. Wang, N.X. Wang, H.X. Guo, W.H. Zhang, X.T. Li, S.L. Ji, Q.F. An, Covalent organic frameworks hybird membrane with optimized mass transport nanochannel for aromatic/aliphatic mixture pervaporation, *J. Membr. Sci.* 598 (2020) 117652.
[31] C. Li, J. Li, W.H. Zhang, N.X. Wang, S.L. Ji, Q.F. An, Enhanced permeance for PDMS organic solvent nanofiltration membranes using modified mesoporous silica nanoparticles, *J. Membr. Sci.* 612 (2020) 118257.
[32] C. Li, J. Li, T.X. Cao, P. Cai, N.X. Wang, Q.F. An, Impact of crosslinking on organic solvent nanofiltration performance in polydimethylsiloxane composite membrane: Probed by *in-situ* low-field nuclear magnetic resonance spectroscopy, *J. Membr. Sci.* 633 (2021) 119382.
[33] W.H. Zhang, M.J. Yin, Q. Zhao, C.G. Jin, N.X. Wang, S.L. Ji, C.L. Ritt, M. Elimelech, Q.F. An, Graphene oxide membranes with stable porous structure for ultrafast water transport, *Nat. Nanotechnol.* 16 (3) (2021) 337–343.
[34] W.S. Sun, M.J. Yin, W.H. Zhang, S. Li, N.X. Wang, Q.F. An, Tailor-made microstructures lead to high-performance robust PEO membrane for CO_2 capture via green fabrication technique, *Green Energy Environ.* 8 (5) (2023) 1389–1397.
[35] Y.K. Ong, G.M. Shi, N.L. Le, Y.P. Tang, J. Zuo, S.P. Nunes, T.S. Chung, Recent membrane development for pervaporation processes, *Prog. Polym. Sci.* 57 (2016) 1–31.
[36] G.Y. Dong, Y.T. Zhang, X.C. Pang, M. Guo, N. Moriyama, H. Nagasawa, M. Kanezashi, T. Tsuru, Sub-nanometer scale tailoring of the microstructures of composite organosilica membranes for efficient pervaporation of toluene/n-heptane mixtures, *J. Membr. Sci.* 672 (2023) 121469.
[37] C. González-Galán, A. Luna-Triguero, J.M. Vicent-Luna, A.P. Zaderenko, A. Sławek, R. Sánchez-de-Armas, S. Calero, Exploiting the π-bonding for the separation of benzene and cyclohexane in zeolites, *Chem. Eng. J.* 398 (2020) 125678.
[38] L. Wang, S.L. Ji, N.X. Wang, R. Zhang, G.J. Zhang, J.R. Li, One-step self-assembly fabrication of amphiphilic hyperbranched polymer composite membrane from aqueous emulsion for dye desalination, *J. Membr. Sci.* 452 (2014) 143–151.
[39] T.P. Wang, D.Y. Kang, Highly selective mixed-matrix membranes with layered fillers for molecular separation, *J. Membr. Sci.* 497 (2016) 394–401.